

Electron Recoil via Sample Momentum Transfer under Optical Excitation

Akira Yasuhara¹, Yamato Kirii², Takumi Sannomiya^{2,*}

¹JEOL Ltd., 3-1-2 Musashino, Akishima, Tokyo, 196-8558, Japan.

² Department of Materials Science and Engineering, School of Materials and Chemical Technologies, Institute of Science Tokyo, 4259 Nagatsuta, Midoriku, Yokohama, 226-8503, Japan

ABSTRACT.

The interaction between free electrons and optical modes underlies a variety of quantum and nanoscale light–matter phenomena, yet the associated momentum exchange with the sample largely remained overlooked. Here, we experimentally demonstrate the momentum transfer from free electrons to planar samples during optical mode excitation using momentum-resolved electron energy-loss spectroscopy. The momentum transfer to the sample modifies the apparent dispersion relation which is significant when the planer sample is tilted. Under specific conditions, the sample receives momentum opposite to the electron beam direction.

Coherent optical excitation by free electrons has attracted renewed interest for its potential to reveal quantum correlations and entanglement between electrons and photons or quasiparticles generated through the electromagnetic interaction [1–5]. Such processes, governed by energy or/and momentum conservation, form the basis for a range of emerging concepts in free-electron quantum optics, including quantum state generation [6–8], quantum measurement [9], or signal enhancement [10,11]. To excite optical modes and emit photons or quasiparticles, an electron typically interacts with a material sample that mediates the electromagnetic interaction and imposed energy–momentum exchange. In such interactions, part of the electron’s momentum may be transferred to the sample to satisfy momentum conservation [12–14]. In contrast to energy entanglement, which can be probed by spectral selection of correlated photons and electrons, momentum-entangled interactions have been investigated using planar samples to minimize the complexity arising from in-plane momentum transfer to nanostructured materials [14,15]. Nevertheless, even in planar geometries, momentum transfer perpendicular to the surface occurs to ensure total momentum conservation. However, quantitative manifestation of momentum transfer to the sample through electron recoil during optical excitation has not yet been experimentally investigated.

Here, we show how such momentum transfer occurs in planar samples through the excitation of in-plane optical modes and how it modifies the apparent dispersion relation using the momentum-resolved electron energy-loss spectroscopy (qEELS) based on

transmission electron microscopy (TEM). [16–18]. We further demonstrate that under specific conditions, the optical excitation can induce a recoil effect in which the sample effectively receives momentum directed opposite to the incident electron beam. For this demonstration, we prepared a specimen consisting of metal films deposited on an amorphous silicon nitride (Si_3N_4) membrane of 200 nm thick, as shown in Fig. 1a. The membrane has an array of holes with a periodicity of 200 nm, which works a measure for the sample tilt and the scale calibration as we discuss later. (Fig. 1b) The sample was tilted by angle φ around the y axis, as indicated in the figure. The

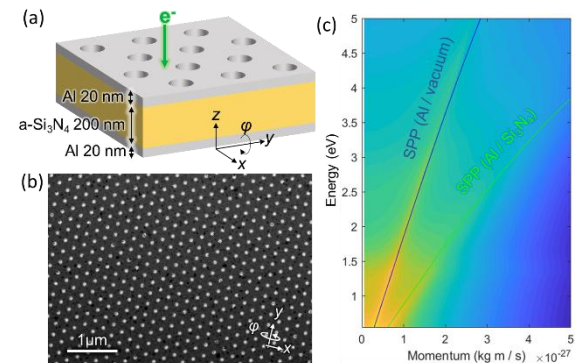


FIG 1. (a) Illustration of the sample and coordinate. (b) TEM bright field image of the sample. (c) Calculated dispersion plot, where the determinant inverse of the boundary condition coefficient matrix is plotted as the contour map. The SPP DRs at a single interface are overlaid as lines.

*Contact author: sannomiya.t.aa@m.titech.ac.jp

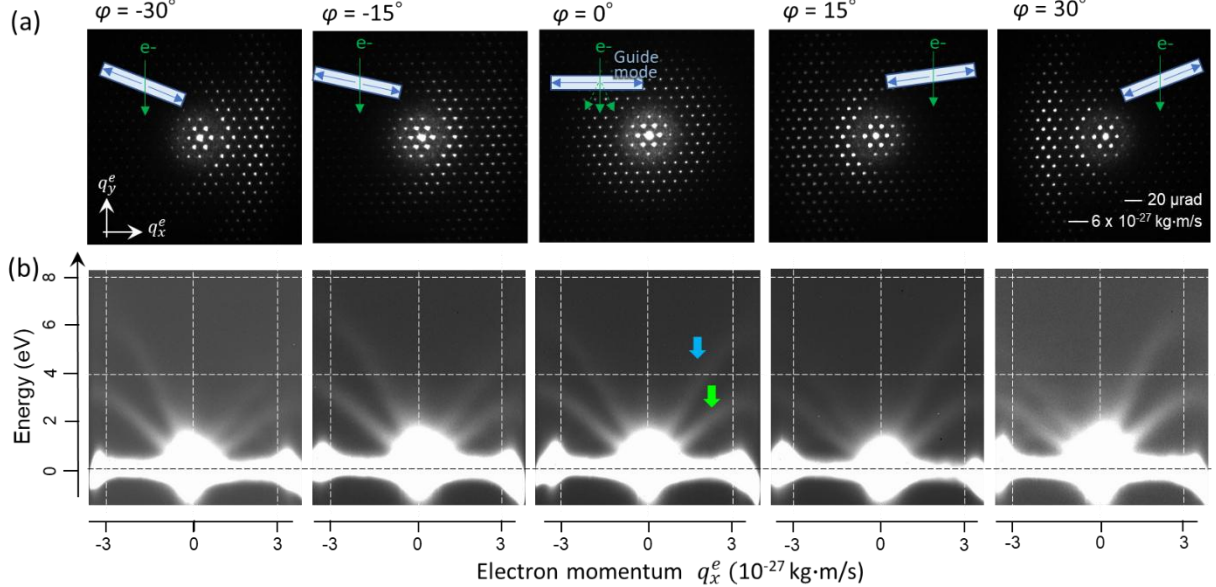


FIG 2. (a) Elastic electron diffraction patterns with different sample tilt angles $\varphi = 0, \pm 15, \pm 30^\circ$ around the y axis. (b) DRs obtained by qEELS at corresponding sample tilt angles. The DR lines of SPPs at the vacuum and Si_3N_4 interfaces are indicated by blue and green arrows in the middle panel ($\varphi = 0^\circ$)

expected dispersion relation (DR) of the optical modes supported in such a membrane is described in Figure 1c. [19] The surface plasmon polaritons (SPPs) on both sides of the aluminum (Al) films are dominant, which are also indicated by the continuous lines of single-interface DRs. [20] The lossy nature of Si_3N_4 of the used specimen well separates the optical coupling between the two metal films as well as damps the dielectric guide mode [21–23]. (see Supplemental Material).

To evaluate the DRs and the momentum transfer from the electron to the sample, low-angle diffraction patterns and qEELS spectra are obtained at different sample tilt angles, as shown in Fig.2a. The measurement was all performed at 200 kV acceleration using a JEM-F200 (JEOL Ltd., Japan) instrument equipped with a GIF Continuum ER (Gatan Inc., USA). The observed diffraction spots reflect the periodicity of the holes. Without the tilt (Fig.2, middle), where the diffraction pattern intensity is symmetrically distributed, the DR curves of the electrons in Fig.2b nicely matches the expected DR curves of SPPs in Fig. 1c. The SPP DRs are distributed symmetrically on both positive and negative sides of the horizontal momentum axis.

By tilting the sample, the diffraction pattern intensities in Fig. 2a become asymmetric along the q_x direction with non-concentric dark ring patterns similar to Laue zones in 3D crystals. [24,25] In the qEELS results in Fig.2b, the observed electron DR looks also asymmetric by the sample tilt, showing “inclined” DR

lines, which seemingly not directly correspond to the pure SPP DRs.

To elucidate this apparent electron DR modulation by the sample tilt, we now consider the momentum transfer to the sample, which is schematically illustrated in Fig.3. For the elastic scattering, one can only consider the momentum transfer to the lattice whereas for the inelastic scattering optical guide mode should be considered (Fig.3a). Because the sample is thin, the reciprocal lattice is elongated in the z direction, also forming the fringe patterns in the z direction due to the finite sample thickness (Fig. 3b). [26] For the elastic scattering, intersections of the reciprocal lattice and the Ewald sphere (red lines in Fig.3b) corresponds to the momentum conservation. Due to the curvature, the Ewald sphere goes across the z -fringe node positions, forming the Laue zone-like dark rings in the diffraction patterns found in Fig.2a. For the inelastic scattering, where the length of the electron momentum vector changes, the momentum conservation of the entire system including optical modes and the sample should be considered, as shown in Fig.3c. Here we consider only a single particle (SPP, or guide mode) generated by one electron, which is reasonable for this system. [14,27] The momentum vectors of the scattered electron (e.g. q_+^e), optical mode (q_+^p), and sample (q_+^s) are added to meet the initial momentum of the electron (q_0^e). Since the optical guide mode (SPP) is supported by the thin sample, this mode can be described as a cylinder

*Contact author: sannomiya.t.aa@m.titech.ac.jp

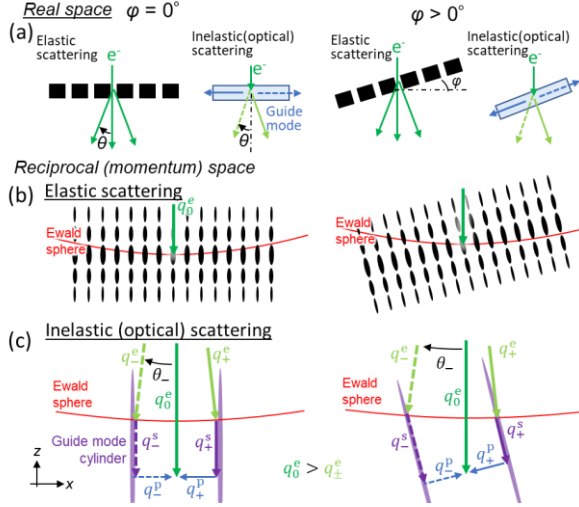


FIG. 3. (a) Illustrations of the diffraction (left) without and (right) with sample tilts. (b) Reciprocal space describing the elastic diffraction by the periodic holes structures in the membrane. (c) Reciprocal space describing the inelastic scattering due to optical mode on the film plane.

elongated in the z -direction in the reciprocal (momentum) space, as described as diffuse violet lines in Fig.3c. (see also SM for the 3D representation) [23] Without the sample tilt ($\varphi = 0^\circ$), this scattering process is symmetric around the z axis.

By tilting the sample ($\varphi > 0$), the reciprocal lattice points related to the periodic holes, as well as the optical mode cylinder for the inelastic scattering, are inclined, as described in the right panels of Fig.3. For the elastic scattering, the sample tilt results in the asymmetric intersections of the Ewald sphere, which explains the asymmetric intensity distributions of Fig.2a in the tilted conditions. Also in the inelastic scattering process by optical excitation, the inclined guide mode cylinder results in the asymmetric intersections with the Ewald sphere, as described in the right panel of Fig.3c. This asymmetry exerts a larger in-plane momentum of electrons in the negative side (q_-^e) and a smaller in the positive side (q_+^e), which induces apparent “inclined” DR of electrons, as in the experiment of Fig.2b.

The cross-section of the Ewald sphere and the optical mode cylinder at a given energy (Fig. 3c) can also be experimentally confirmed by energy-filtered diffraction patterns, as shown in Fig. 4 (obtained in a planer area without lattice structure to avoid dispersion cone overlaps). The dispersion circles, which is concentric without the sample tilt (Fig.4a), become distorted and displaced from the center by tilting the sample (Fig.4b).

This scattering process can be more quantitatively described using the momenta of the electron q^e , optical

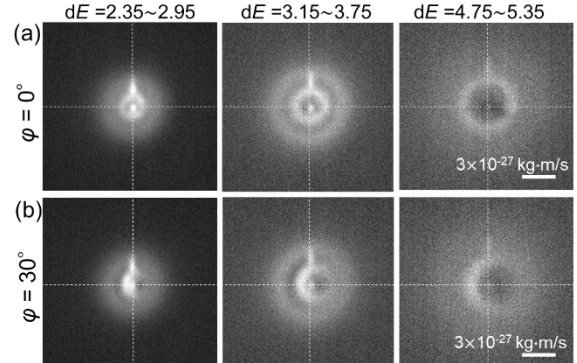


FIG. 4. Energy-filtered diffraction patterns (a) without and (b) with sample tilts, obtained at a planer position without lattice structures.

mode q^p , and sample q^s after scattering with the sampled tilt $\varphi > 0$. Here we only consider the deflection in the q^e side with the electron deflection angle θ_- which is enhanced by launching the optical mode (left-hand side of each illustration in Fig. 3c). The opposite scattering side can be obtained by flipping the sign of φ . The momentum conservations are expressed as $q_-^e \sin \theta = q_-^s \sin \varphi + q^p \cos \varphi$ for the x direction, and $q_0^e = q_-^e \cos \theta + q_-^s \cos \varphi - q^p \sin \varphi$ for the z direction. q_0^e is the initial momentum of the incident electron. When the DR of the optical mode is known, as in Fig.1, the electron scattering angle θ and the transferred momentum to the sample q_-^s can be calculated. For sufficiently small θ ($\ll 1$), which is the case for optical excitations, θ and q^s are expressed as:

$$\theta_- = \frac{1}{q_-^e} \{ q^p \cos \varphi + (\Delta q^e + q^p \sin \varphi) \tan \varphi \}, \quad (1)$$

$$q_-^s = \frac{1}{\cos \varphi} (\Delta q^e + q^p \sin \varphi). \quad (2)$$

Here $\Delta q^e = q_0^e - q_\pm^e$ is the momentum amplitude change of the electron by inelastic scattering. We note that q^s vector is always perpendicular to the sample surface.

The calculated electron DRs, corresponding to the x component of the electron momentum $q_x^e = q_\pm^s \sin \theta_\pm$ at a given loss energy, are shown in Fig.5a for different sample tilt angles. The dispersion branches for SPPs in the positive or negative x directions (subscript signs in Fig.3 and Eqs.1,2) are indicated by circles and colored for the vacuum (blue) or Si_3N_4 (green) interfaces. The calculation nicely reproduces the experimentally observed electron DR of Fig.2b showing the inclined curves by the sample tilt. The transferred momentum to the sample can also be calculated from Eq (2), as plotted in Fig.5b-e for different tilt conditions. By tilting the sample, in-plane momentum q_x^s is introduced to the sample (Fig. 5b,d), which causes the inclination of the apparent DR of the electron (Fig. 5a).

*Contact author: sannomiya.t.aa@m.titech.ac.jp

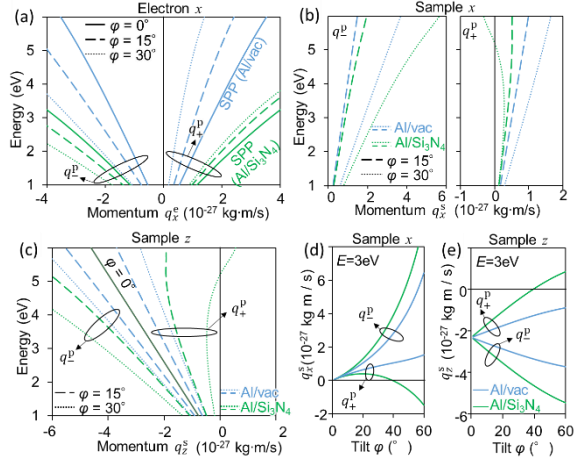


FIG 5. (a) Calculated in-plane electron DR with different tilt angles. (b,c) Transferred momentum to the sample in the (b) in-plane x (plots separated for two scattering branches) and (c) out-of-plane z directions. (d,e) Transferred momentum plotted as functions of the sample tilt angle.

The z momentum introduced to the sample is downward ($q_z^s < 0$ in Fig.5c,e) in most conditions, which is natural since the fast electron is pushing down the sample. However, for the SPPs on Si_3N_4 with high angle tilts, the sample can be pushed upwards ($q_z^s > 0$) against the electron traveling direction, as a result

of launching a SPP downwards (e.g. $\varphi = 30^\circ$, $E > 5$ eV, $\text{Al}/\text{Si}_3\text{N}_4$, q_+^p branch in Fig.4c, or $\varphi > 40^\circ$ in Fig.4e). This condition coincides with the sample momentum sign change in the x direction (Fig.5b,d). Such a counter push of the sample cannot happen for free-space photon generations since the free electron momentum change is larger than that of free photons with the same kinetic energy. SPPs of high momenta, such as those at dielectric/metal interfaces, with high sample tilt angle is required to fulfill this condition such that the total momentum of the electron, sample, and guide mode is conserved. (Higher tilt conditions are described in Supplemental Material [23])

In conclusion, we have demonstrated the modulation of the DR obtained in qEELS measurement by transferring the momentum to the sample through the sample tilt. Such momentum transfer to the sample is important to analyze the correlation, including entanglement, of the electron and electromagnetic mode. One can also possibly consider the entanglement with the sample [28] or mechanically drive the sample by controlling the electromagnetic modes. [29]

ACKNOWLEDGMENTS

This work is supported by JST CREST JPMJCR25I3, FOREST JPMJFR213J, and JSPS Kakenhi 24H00400.

- [1] A. Feist, K. E. Echternkamp, J. Schauss, S. V. Yalunin, S. Schäfer, and C. Ropers, Quantum coherent optical phase modulation in an ultrafast transmission electron microscope, *Nature* **521**, 200 (2015).
- [2] O. Kfir, Entanglements of Electrons and Cavity Photons in the Strong-Coupling Regime, *Phys. Rev. Lett.* **123**, 103602 (2019).
- [3] G. Huang, N. J. Engelsen, O. Kfir, C. Ropers, and T. J. Kippenberg, Electron-Photon Quantum State Heralding Using Photonic Integrated Circuits, *PRX Quantum* **4**, 020351 (2023).
- [4] F. J. García de Abajo et al., Roadmap for Quantum Nanophotonics with Free Electrons, *ACS Photonics* **12**, 4760 (2025).
- [5] R. Ruimy, A. Karnieli, and I. Kaminer, Free-electron quantum optics, *Nat. Phys.* **21**, 193 (2025).
- [6] X. Bendaña, A. Polman, and F. J. García de Abajo, Single-Photon Generation by Electron Beams, *Nano Lett.* **11**, 5099 (2011).
- [7] R. Dahan et al., Imprinting the quantum statistics of photons on free electrons, *Science* **373**, eabj7128 (2021).
- [8] G. Arend et al., Electrons herald non-classical light, *Nat. Phys.* **1** (2025).
- [9] J.-W. Henke, H. Jeng, and C. Ropers, Probing electron-photon entanglement using a quantum eraser, *Phys. Rev. A* **111**, 012610 (2025).
- [10] A. Feist et al., Cavity-mediated electron-photon pairs, *Science* **377**, 777 (2022).
- [11] N. Varkentina et al., Cathodoluminescence excitation spectroscopy: Nanoscale imaging of excitation pathways, *Sci. Adv.* **8**, eabq4947 (2022).
- [12] G. Baranes, R. Ruimy, A. Gorlach, and I. Kaminer, Free electrons can induce entanglement between photons, *Npj Quantum Inf.* **8**, 32 (2022).
- [13] T. P. Rasmussen, Á. R. Echarri, J. D. Cox, and F. J. G. de Abajo, Generation of entangled waveguided photon pairs by free electrons, *Sci. Adv.* **10**, eadn6312 (2024).
- [14] A. Preimesberger, D. Hornof, T. Dorfner, T. Schachinger, M. Hrtoň, A. Konečná, and P. Haslinger, Exploring Single-Photon Recoil on Free Electrons, *Phys. Rev. Lett.* **134**, 096901 (2025).

*Contact author: sannomiya.t.aa@m.titech.ac.jp

- [15] S. Yanagimoto, N. Yamamoto, T. Yuge, T. Sannomiya, and K. Akiba, Unveiling the nature of cathodoluminescence from photon statistics, *Commun. Phys.* **8**, 56 (2025).
- [16] H. Saito and H. Kurata, Formation of a hybrid plasmonic waveguide mode probed by dispersion measurement, *J. Appl. Phys.* **117**, 133107 (2015).
- [17] A. Yasuhara, M. Shibata, W. Yamamoto, I. Machfuudzoh, S. Yanagimoto, and T. Sannomiya, Momentum-resolved EELS and CL study on 1D-plasmonic crystal prepared by FIB method, *Microscopy* **73**, 473 (2024).
- [18] M. Hayashida, M. T. Schreiber, H. Müller, Y. Taniguchi, J. Canlas, C. Soong, K. Cui, R. Egerton, and M. Malac, Momentum-dispersion calibration and measurement of a surface layer dielectric constant using momentum-resolved electron energy-loss spectroscopy in the optical region, *Micron* 103907 (2025).
- [19] Y. Ikenoya, M. Susa, J. Shi, Y. Nakamura, A. B. Dahlin, and T. Sannomiya, Optical Resonances in Short-Range Ordered Nanoholes in Ultrathin Aluminum/Aluminum Nitride Multilayers, *J. Phys. Chem. C* **117**, 6373 (2013).
- [20] E. D. Palik, *Handbook of Optical Constants of Solids* (Academic Press, 1998).
- [21] H. R. Philipp, Optical Properties of Silicon Nitride, *J. Electrochem. Soc.* **120**, 295 (1973).
- [22] J. Kischkat et al., Mid-infrared optical properties of thin films of aluminum oxide, titanium dioxide, silicon dioxide, aluminum nitride, and silicon nitride, *Appl. Opt.* **51**, 6789 (2012).
- [23] See Supplemental Material for the Details of DR Calculation, 3D Representation of the Momentum Space, and High Tilt Angle Conditions.
- [24] R. Bergsten, Optical simulation of electron diffraction of thin crystals, *JOSA* **64**, 1309 (1974).
- [25] L. Reimer, *Transmission Electron Microscopy: Physics of Image Formation* (Springer, New York, NY, 1997).
- [26] H. M. Otte, J. Dash, and H. F. Schaake, *Electron Microscopy and Diffraction of Thin Films: Interpretation and Correlation of Images and Diffraction Patterns*, *Phys. Status Solidi B* **5**, 527 (1964).
- [27] F. J. García de Abajo, Optical excitations in electron microscopy, *Rev. Mod. Phys.* **82**, 209 (2010).
- [28] A. Konečná, F. Iyikanat, and F. J. García de Abajo, Entangling free electrons and optical excitations, *Sci. Adv.* **8**, eab07853 (2022).
- [29] Y. Y. Tanaka, P. Albella, M. Rahmani, V. Giannini, S. A. Maier, and T. Shimura, Plasmonic linear nanomotor using lateral optical forces, *Sci. Adv.* **6**, eabc3726 (2020).

*Contact author: sannomiya.t.aa@m.titech.ac.jp

Supplemental Material for

Electron Recoil via Sample Momentum Transfer under Optical Excitation

Akira Yasuhara¹, Yamato Kirii², Takumi Sannomiya^{2,*}

¹JEOL Ltd., 3-1-2 Musashino, Akishima, Tokyo, 196-8558, Japan.

² Department of Materials Science and Engineering, School of Materials and Chemical Technologies, Institute of Science Tokyo, 4259 Nagatsuta, Midoriku, Yokohama, 226-8503, Japan

S1. Dispersion relation calculation

For the dispersion relation calculation, constant refractive index of $2.1 + 0.2i$ was used for the silicon nitride films and dispersive dielectric function was used for the aluminum.[20] The calculation method for the multilayer (vacuum/Al/Si₃N₄/Al/vacuum) is shown in the previous work [19]. We used the inverse of the determinant of the calculation matrix X , which expresses the series of boundary conditions, for the plot Fig.1c. For the single interface DR plot, commonly used formulation of $k = \frac{\omega}{c} \sqrt{\frac{\varepsilon_1 \varepsilon_2}{\varepsilon_1 + \varepsilon_2}}$ is used. (k : wavenumber, ω : angular frequency, c : light speed, ε_1 : dielectric constant of the medium, ε_2 : dielectric function of the metal.).

S2. 3D representation of the momentum space

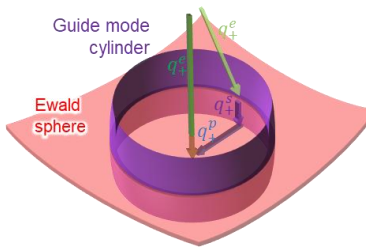


Fig.S1. 3D representation of the guide mode cylinder crossing the Ewald sphere.

*Contact author: sannomiya.t.aa@m.titech.ac.jp

S3. High tilt results

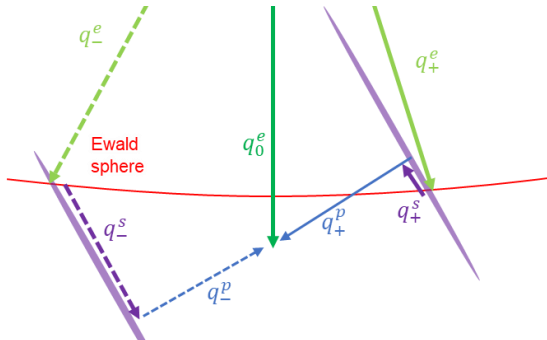


Fig.S2 Illustration of momentum space with a large guide mode momentum q^p and high sample tilt angle φ .
The momentum direction of the sample q_+^s may flip.

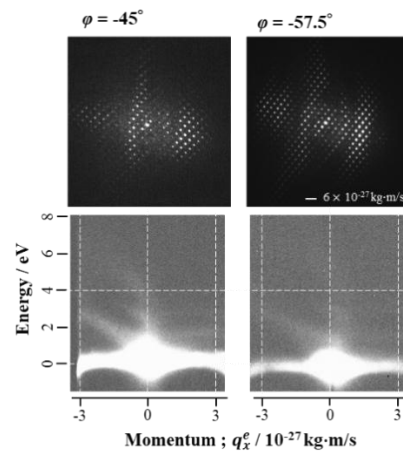


Fig.S3. qEELS measurement at high sample tilt angles. The dispersion becomes more difficult to recognize because of the increased effective sample thickness as well as intersection with the lattice modes and the thickness fringes.

*Contact author: sannomiya.t.aa@m.titech.ac.jp